J. Phys. C: Solid St. Phys., 13 (1980) 213–31. Printed in Great Britain.

# Magnetic properties of the $Ho_cY_{1-c}Sb$ system

J Jensen†, N Hessel Andersen† and O Vogt‡

† Physics Laboratory I, H C Ørsted Institute, University of Copenhagen, Denmark

‡ Laboratorium für Festkörperphysik, ETH, Zürich, Switzerland

Received 21 March 1979

**Abstract.** Magnetisation measurements on the cubic alloy system $Ho_cY_{1-c}Sb$ at 1·6 K are presented. The results obtained when the field is applied along the easy [100] axis show the presence of an intermediate phase between the high-field, ferromagnetic and the low-field, antiferromagnetic phase in the Ho-rich alloys. First-order transitions are observed when the field is along the hard [110] or [111] axes. The variation of the Néel temperature, $T_N$, with Ho concentration, $c$, has been determined by magnetisation and electrical resistivity measurements down to $c = 0{\cdot}4$, and the paramagnetic susceptibility has been measured as a function of temperature and concentration. A molecular-field model is developed which describes accurately most of the magnetic properties of the $Ho_cY_{1-c}Sb$ system. The two-sublattice calculations presented include the effects of isotropic and anisotropic bilinear pair interactions, acoustic and optical quadrupole couplings and the crystal field. The intermediate phase, present in an applied field along [100] at 1·6 K, is predicted to be very similar to the flopside phase of HoP. At low temperatures, the direction of magnetisation is close to a [100] direction but is found to tilt with increasing temperature in a similar way to that observed in DySb. The model predicts the occurrence of a second-order phase transition at $T_N = 5{\cdot}7$ K in HoSb followed by a tricritical-like transition at 5·4 K. This explains the anomalous behaviour of the magnetic neutron scattering observed by Taub and Parente, and it is consistent with heat capacity measurements.

## 1. Introduction

The rare-earth monopnictides crystallise in the simple NaCl structure and their magnetic properties are of considerable interest because the crystal-field effects dominate, but the two-ion couplings are sufficiently strong to give rise to collective phenomena at low temperatures. The rare-earth antimonides are metals (Hessel Andersen *et al* 1979a), and the conduction electrons are coupled to the magnetic 4f electrons of the rare-earth ions, as manifested, for example, in the temperature-dependent resistivity. The exchange interaction between the 4f electrons and the conduction electrons introduces an indirect coupling between the magnetic ions. To a first approximation this coupling is isotropic, but the presence of anisotropic terms is predicted whenever the 4f electrons possess a non-vanishing orbital momentum (Kaplan and Lyons 1963). These anisotropic terms are, in the present context, entirely equivalent to the magnetic dipole coupling. The isotropic exchange coupling is relatively weak in these compounds, whereas the magnetic moments are large, implying that the microscopic dipole field might be of importance, as first realised by Trammell (1963). The Coulomb scattering of the conduction electrons,

0022-3719/80/020213+19 $01.00 © 1980 The Institute of Physics 

which produces indirect quadrupole–quadrupole couplings between the ions, seems to be just as important as the exchange scattering for explaining the magnetic contributions to the resistivity of TmSb (Hessel Andersen and Vogt 1979). Extending this result to HoSb we may expect that the electronic quadrupole coupling contributes to the magnetic energy by terms of the order of 10% of the exchange contribution. This is of the same order of magnitude as the quadrupole couplings induced by the magnetoelastic interaction in HoSb, due to the strain dependence of the crystal field (Mullen *et al* 1974, Lüthi *et al* 1977).

An estimate of the crystal-field parameters of HoSb may be obtained by interpolation between those determined in other rare-earth antimonides. This procedure gives a value of the parameter $x$ (Lea *et al* 1962) which is close to the value $x_c = \frac{6}{7}$, at which the six (lowest) levels, consisting of the $\Gamma_1$, $\Gamma_4^{(2)}$, and $\Gamma_3^{(2)}$ become degenerate. This arrangement of the crystal-field levels leads to a number of special magnetic properties first considered by Uffer *et al* (1974) and later discussed at length by Kim *et al* (1975, 1976).

HoSb orders antiferromagnetically with a Néel temperature, $T_N$, of about 5·4 K. Neutron diffraction measurements (Taub and Parente 1975) indicate a continuous variation of the order parameter, corresponding to a second-order transition, but the results show an anomalously large intensity of magnetically scattered neutrons above 5·4 K. HoSb is a type-II antiferromagnet composed of ferromagnetic (111) planes, with the moments of adjacent planes oriented antiparallel. At low temperatures the magnetic moments point along a [100] axis (Child *et al* 1963), but it was suggested that the moments were tilted slightly in a direction away from the cube diagonal.

Here we shall report an extensive study of the ground state properties of $Ho_cY_{1-c}Sb$. In accordance with the virtual crystal approximation, we assume that the random replacement of Ho ions with the fraction $1 - c$ of non-magnetic Y ions only introduces a uniform scaling, proportional to $c$, of the interaction between the Ho ions, leaving the crystal-field parameters unchanged. The analysis of the magnetic part of the resistivity in the equivalent system of $Tb_cY_{1-c}Sb$ by Hessel Andersen *et al* (1979a) indicates that this simple model is a valid approximation. The magnetisation measurements performed on $Ho_cY_{1-c}Sb$ at 1·6 K, with the field applied along the three main axes, which we shall present in § 2, show clearly the importance of the anisotropic two-ion couplings. Combined with the other experiments these informative results made it possible to establish a detailed model for the magnetic properties of HoSb. In § 3 we present the two-sublattice model and the details of the molecular-field (MF) calculations used in the comparison with experiments. Finally, we make some concluding remarks in § 4, and discuss the implications of the present model for the understanding of other rare-earth monopnictides.

## 2. Experiments

Single crystals of $Ho_cY_{1-c}Sb$ were prepared in a way similar to those of $Tb_cY_{1-c}Sb$, as reported by Hessel Andersen *et al* (1979a). The crystals were examined by the electron microprobe technique. Contrary to the case of the Tb system, the final concentration of the Ho ions always turned out to be close to the starting value, and no concentration gradients over the samples were observed. The concentration of Ho ions in the different crystals was chosen so as to cover uniformly the whole range $1 \geqslant c > 0$.

The initial susceptibility was determined experimentally by the Faraday method in the temperature range between room temperature and 1·6 K on a sample consisting of

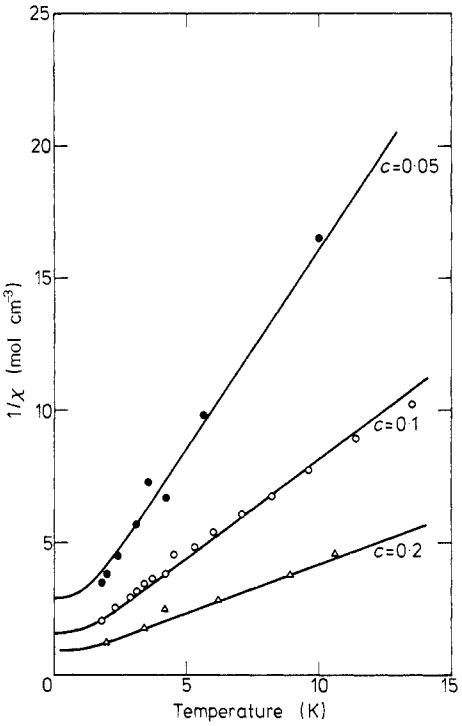


**Figure 1.** The inverse susceptibility of $Ho_cY_{1-c}Sb$ in the dilute cases and at low temperatures. The full curves in this and the following figures display the theoretical results.

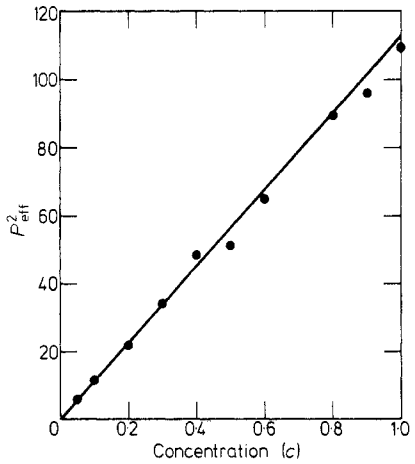


**Figure 2.** The slope of the inverse susceptibility versus $T$ as a function of the concentration of Ho ions. $1/\chi$ is found to depend linearly on $T$ in the range 10–300 K and the slope is expressed in terms of the square of the effective number of Bohr magnetons per ionic unit ($Ho_cY_{1-c}Sb$).

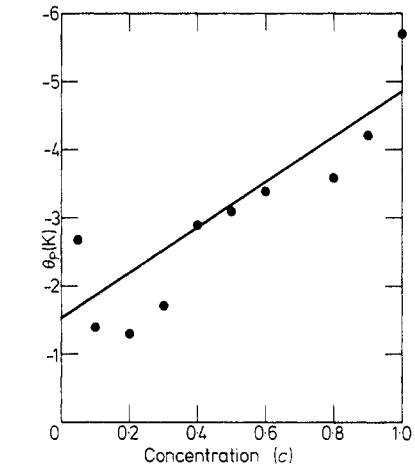


**Figure 3.** The paramagnetic Curie temperature, $\theta_p$, as a function of $c$ determined by the linear temperature dependence of $1/\chi$ in the range 10–300 K. $\theta_p$ is determined experimentally with an uncertainty of 1 K at all the concentrations.

several single crystals. In figure 1 are shown the low-temperature results for the most dilute samples ($c$ = 0·05, 0·1, and 0·2) reflecting almost exclusively the single-ion behaviour of the Ho ions. The full curves on this figure and all the following ones are the results of the calculations presented in the next section. Within the experimental accuracy, the inverse susceptibility was found to be a linear function of $T$ between 10–300 K for all the values of $c$. In figure 2 we have plotted the slope of the inverse susceptibility versus $T$, converted to the square of the effective number of Bohr magnetons per ionic unit,

$P^2_{\text{eff}}$. We note that the result is very close to that expected for free Ho ions, namely

$$P^2_{\text{free ion}} = cg^2J(J+1) = 112{\cdot}5c$$

with $g = \frac{5}{4}$ and $J = 8$ for $Ho^{3+}$. The other quantity which characterises the linear part of the inverse susceptibility is the paramagnetic Curie temperature, $\theta_p$. The experimental results for $\theta_p$ are displayed in figure 3; the uncertainties are of the order of 1 K in all cases. For the Ho-rich alloys $\theta_p$ is negative, as might be anticipated for an antiferromagnetic system. However, $\theta_p$ does not approach zero in the dilute limit, which can only be interpreted as a genuine crystal-field effect.

The low-temperature results for the susceptibility of the Ho-rich alloys showed clearly the onset of antiferromagnetic ordering by displaying a maximum around the ordering temperature. In order to study this phase in more detail we made systematic measurements of the bulk magnetisation as a function of magnetic field by using a moving sample magnetometer. In figure 4 we show the magnetisation per Ho ion of

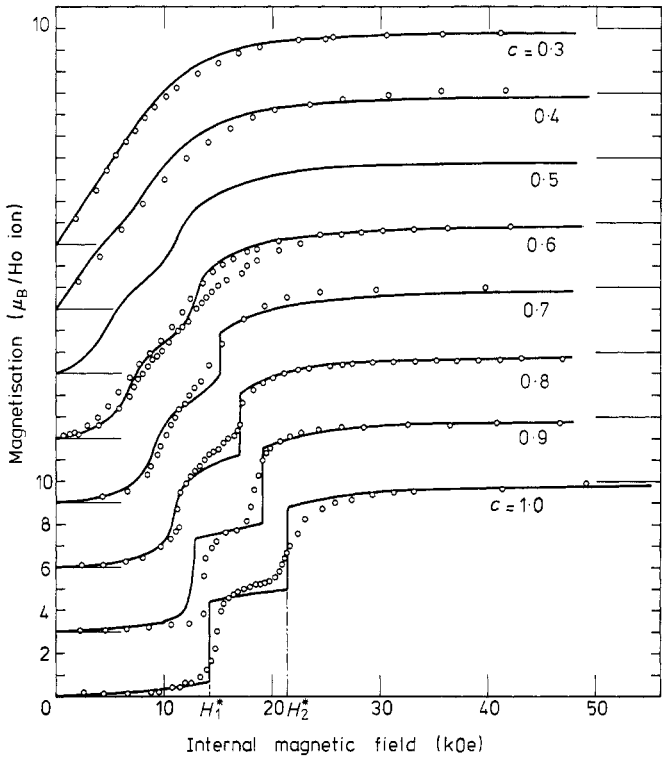


**Figure 4.** The bulk magnetisation of $Ho_cY_{1-c}Sb$ parallel to the field applied along an easy [100] axis as obtained at 1·6 K. The results are expressed in terms of Bohr magnetons per Ho ion. For clarity the magnetisation curves for the various values of $c$ are shifted by a multiple of $3\mu_B$ with respect to each other. The thin lines indicate the saturation value of $10\mu_B$ for the different concentrations. The experimental results for $c = 0{\cdot}5$ are omitted, because it was not possible to produce single crystals of sufficient quality in this case. $H_1^*$ and $H_2^*$ show the positions of the two first-order transitions calculated to occur in HoSb.

At fields smaller than $H_1^*$ the moments on the two sublattices both have a large component perpendicular and a small one parallel to the field, the perpendicular components being oriented antiparallel. The phase present above $H_2^*$ is calculated to be purely ferromagnetic. According to the calculations the stable configuration in HoSb at the intermediate fields is the flopside spin structure of HoP, but slightly distorted.

$Ho_cY_{1-c}Sb$, parallel to the field applied along an easy [100] direction at 1·6 K. The results are given for values of $c$ ranging from 0·3 to 1·0. For clarity the magnetisation curves for the different values of $c$ have been shifted by a multiple of $3\mu_B$ with respect to each other. The thin lines indicate the saturation value of $10\mu_B$ for the different concentrations. The experimental results obtained for $c$ less than 0·3 are not shown. Except for a small change of the initial susceptibility, as determined from figure 1, these dilute crystals gave results which were identical to those obtained for $c = 0{\cdot}3$.

The most remarkable feature of these magnetisation curves is the indication of an intermediate phase in the Ho-rich samples, in which the magnetisation is close to $5\mu_B$/ion, i.e. half the saturation value. It is very tempting to associate this phase with the flopside spin structure of HoP, which was determined from neutron diffraction measurements by Child *et al* (1963). In this structure, the moments are directed along a [100] direction, and the adjacent ferromagnetic (111) planes have the moment directions at right angles to each other. Therefore there is a net ferromagnetic component of the moments parallel to a [110] direction and a net antiferromagnetic one perpendicular to that direction. As discussed in the Introduction, the value of the crystal-field parameter $x$ is presumably close to $x_c = \frac{6}{7}$ in HoSb, which is also the case for the Ho ions in HoP (see for instance Furrer and Kaldis 1975). If $x = x_c$ a very simple basis may be chosen for the wavefunctions of the six degenerate levels of the crystal-field Hamiltonian, namely $|J_{z'} = J\rangle$ where $z'$ is parallel to any of the six equivalent [001] directions (Kim *et al* 1975). This means that in the limit of zero temperature the moments in the ordered phases of HoSb or HoP are strongly confined to be along a [100] direction and to be of maximum magnitude, corresponding to an ionic ground state close to one of the $|J_{z'} = J\rangle$ states. As a first approximation for HoSb we may assume the two constraints to be strictly fulfilled, and $T = 1{\cdot}6$ K may be considered as being close to the zero temperature limit (for $c = 1$). In terms of this simplified model the magnetisation curve in figure 4 for $c = 1$ would consist of entirely straight lines, the moment per Ho ion parallel to the field being equal to 0, $5\mu_B$, or $10\mu_B$ in the respective cases of the antiferromagnetic, the flopside, or the ferromagnetic phases, which corresponds quite well to the observed behaviour. In this model the two values of the field, $H_1^*$ and $H_2^*$, separating the three phases are simply related to the two-ion couplings, as discussed in the next section, and it is easily seen that for vanishing two-ion anisotropy $H_1^*$ and $H_2^*$ coincide, implying that the difference is a direct measure of the two-ion anisotropy energy which favours the flopside structure. Pursuing the model further, we should expect a related behaviour of the magnetisation when the field is applied along a [110] or a [111] direction. In these cases the two possible phases are the antiferromagnetic one and the flopside structure, neglecting the possible existence of more than two different sublattices. The bulk magnetisation should be zero in the first one and for the flopside structure the average ionic moment parallel to the field should be $10/\sqrt{2}\,\mu_B \simeq 7{\cdot}1\mu_B$ and $10/\sqrt{3}\,\mu_B \simeq 5{\cdot}8\mu_B$ when the field is applied along [110] and [111] respectively. Further, the first-order transition between the two phases should occur when the field is equal to $H_3^* = H_1^*/\sqrt{2}$ or $H_4^* = H_1^* \times \sqrt{3}/2$ respectively in the two cases. In figure 5 we show the experimental results for the magnetisation curves obtained for three values of $c$, when the field is applied in the [110] and [111] directions at 1·6 K. The two first-order transitions at $H_3^*$ and $H_4^*$ are clearly resolved in HoSb, and the experimental ratio between the three critical fields: $H_3^*:H_4^*:H_1^*$ of 0·69:0·83:~1 is close to that predicted by the simple model above, namely 0·71:0·87:1, which is also the case with the high-field values of the average moments.

As the final experimental study we have tried to establish the Néel temperature as a

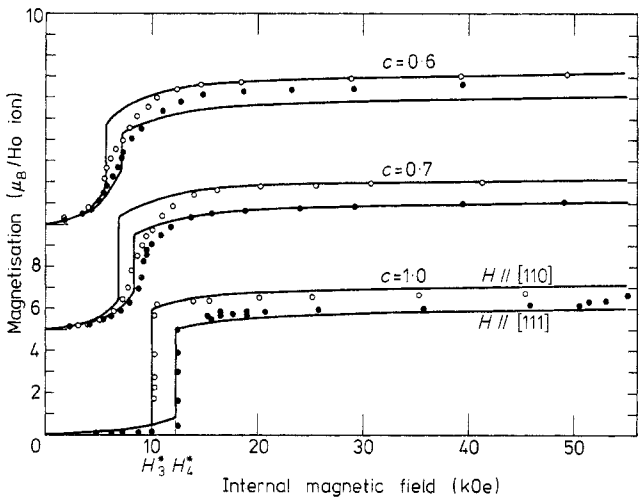


**Figure 5.** The bulk magnetisation of $Ho_cY_{1-c}Sb$ at 1·6 K obtained when the field is applied along the hard [110] and [111] axes. The magnetisation parallel to the field is expressed in Bohr magnetons per Ho ion, and the curves obtained at the three values of $c$ are shifted by $5\mu_B$ with respect to each other. The experimental results obtained with the applied field along [110] or [111] are denoted by open or full circles in the respective cases. $H_3^*$ and $H_4^*$ are the fields at which the transitions between the antiferromagnetic and flopside-like structures are calculated to occur in HoSb.

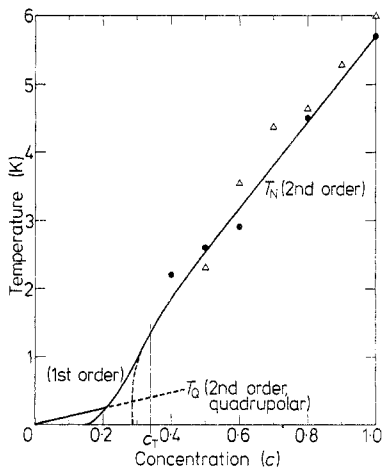


**Figure 6.** The Néel temperature of $Ho_cY_{1-c}Sb$ as a function of $c$. The transition temperature at the different concentrations is determined experimentally by magnetisation and electric resistivity measurements, the results of which are shown by the triangles and the full circles respectively. By extrapolating the linear temperature dependence of the neutron scattering intensity at $\boldsymbol{Q}$, observed in HoSb by Taub and Parente (1975) between 5·4 and 5·6 K, to zero intensity we estimate $T_N$ to be 5·70 ± 0·05 K in HoSb. The full curves display the theoretical results of the MF calculation which predicts the transition to be of second order at concentrations larger than $c_T \simeq 0{\cdot}34$, changing to first order at smaller concentrations. The continuation of the phase-line of the second-order transition is indicated by a broken line. At $c_T$ the system is tricritical. For $c$ smaller than about 0·15 magnetic ordering is no longer possible. In the phase diagram we also indicate the calculated temperature $T_Q$, for the second-order transition to the non-magnetic quadrupolar phase described in the text. This phase is destroyed by the onset of magnetic ordering.

function of the concentration of the Ho ions. In this study we used two methods. The first consisted of measuring the bulk magnetisation at constant value of the applied field as a function of temperature. By extrapolating the temperature at which the maximum occurred for different values of the applied field down to zero field, we obtained the results shown by the triangles in figure 6. As the second method we utilised the very rapid variation of the electric resistivity occurring just around $T_N$, observed also by Taub and Williamson (1973) and Taub *et al* (1974) in pure HoSb, which is similar to that of $Tb_cY_{1-c}Sb$ (Hessel Andersen *et al* 1979a). The results obtained using this method are denoted by the full circles in figure 6. A more detailed account of the resistivity measurements for the various concentrations will be published elsewhere (Hessel Andersen *et al* 1979b). Both the two methods are subject to an uncertainty of the order of a few tenths of a degree, and for the dilute crystals ($c \leqslant 0{\cdot}3$) no sign of the possible occurrence of antiferromagnetic ordering above 1·6 K could be detected.

## 3. Mean-field calculation of the ground-state properties

In the Introduction we argued that various types of interactions were expected to be important for the magnetic properties of $Ho_cY_{1-c}Sb$. As discussed in the preceding section the magnetisation curves in figure 4 clearly indicate the presence of anisotropic couplings between the Ho ions sited on the two different sublattices. Therefore we base our calculations on the following two-ion Hamiltonian:

$$\begin{aligned}\mathscr{H}_{II} = -\tfrac{1}{2}\sum_{i\neq j}\Big[&\mathscr{J}(\boldsymbol{r}_i-\boldsymbol{r}_j)\boldsymbol{J}_i\cdot\boldsymbol{J}_j+\mathscr{J}_D(\boldsymbol{r}_i-\boldsymbol{r}_j)\left[3(\hat{\boldsymbol{r}}_{ij}\cdot\boldsymbol{J}_i)(\hat{\boldsymbol{r}}_{ij}\cdot\boldsymbol{J}_j)-\boldsymbol{J}_i\cdot\boldsymbol{J}_j\right]\\&+K(\boldsymbol{r}_i-\boldsymbol{r}_j)\sum_{m=-2,0,2}\tfrac{1}{4}\left[\tilde{O}_{2,m}(\boldsymbol{J}_i)+\tilde{O}_{2,-m}(\boldsymbol{J}_i)\right]\left[\tilde{O}_{2,m}(\boldsymbol{J}_j)+\tilde{O}_{2,-m}(\boldsymbol{J}_j)\right]\\&+K'(\boldsymbol{r}_i-\boldsymbol{r}_j)\Big(\sum_{m=-1,1}\tilde{O}_{2,m}(\boldsymbol{J}_i)\,\tilde{O}_{2,-m}(\boldsymbol{J}_j)\\&+\tfrac{1}{2}\left[\tilde{O}_{2,2}(\boldsymbol{J}_i)-\tilde{O}_{2,-2}(\boldsymbol{J}_i)\right]\left[\tilde{O}_{2,2}(\boldsymbol{J}_j)-\tilde{O}_{2,-2}(\boldsymbol{J}_j)\right]\Big)\Big].\end{aligned}\tag{1}$$

$\boldsymbol{J}_i$ is the total angular momentum of the Ho ion at the position $\boldsymbol{r}_i$, $\hat{\boldsymbol{r}}_{ij}$ is a unit vector along $\boldsymbol{r}_i-\boldsymbol{r}_j$, $\tilde{O}_{2,m}$ denotes a second rank Racah operator (see for instance Lindgård and Danielsen 1974), and the $x$, $y$, and $z$ axes are along the three crystallographic [001] directions. This Hamiltonian contains the bilinear and biquadratic interactions which might contribute to the MF Hamiltonian of HoSb. Besides the higher-order multipole couplings we neglect only the possible strain dependence of the two-ion terms, which probably are relatively of the same order of magnitude as the strains ($10^{-3}$). The self-consistent MF equations were solved numerically, but in an estimate of the different effects of the interactions, the simple crystal-field model used in the preceding section is of great value. For instance, within this model the expectation value of $(J_\alpha J_\beta)_i^{\alpha\neq\beta}$ is zero. This was not entirely true in the numerical calculations, and instead of neglecting $K'(\boldsymbol{r}_i-\boldsymbol{r}_j)$ we make the somewhat more realistic assumption that

$$K'(\boldsymbol{r}_i-\boldsymbol{r}_j) = -K(\boldsymbol{r}_i-\boldsymbol{r}_j).$$

This choice implies that the quadrupolar coupling becomes particularly simple by being independent of a coordinate transformation within the angular momentum space, and

the quadrupolar part of (1) may be written in the condensed form

$$\sum_{m=-2}^{+2} (-1)^m \tilde{O}_{2,m}(\boldsymbol{J}_i)\, \tilde{O}_{2,-m}(\boldsymbol{J}_j) = \tfrac{3}{2}(\boldsymbol{J}_i \cdot \boldsymbol{J}_j)^2 - \tfrac{1}{2}J^2(J+1)^2.$$

The two-ion Hamiltonian is treated within the molecular-field approximation. A further reduction of the complexity of the problem is attained by assuming that only two different magnetic sublattices are present. This assumption is valid if the different (111) planes within one of the sublattices are coupled ferromagnetically. An estimate shows that the strength of this coupling needs only to be of the order of one tenth of the total ferromagnetic coupling deduced for the ions within one of the sublattices. The MF Hamiltonian for a momentum operator belonging to sublattice 1, $\boldsymbol{J}_1$, can then be written:

$$\mathscr{H}_{\mathrm{MF}}(1) = B_4^0(O_4^0 + 5O_4^4) + B_6^0(O_6^0 - 21O_6^4) - g\mu_{\mathrm{B}}\boldsymbol{H} \cdot \boldsymbol{J}_1 + c[\mathscr{H}_{\mathrm{II}}(1) - \tfrac{1}{2}\langle \mathscr{H}_{\mathrm{II}}(1)\rangle]. \quad (2)$$

The crystal-field part is expressed in terms of the Stevens operators as usual. The cases in which $c$ is less than one are included by scaling the two-ion part with the factor $c$ in accordance with the simplest, virtual-crystal, approximation. The two-ion part of (2) is

$$\begin{aligned}\mathscr{H}_{\mathrm{II}}(1) = {} & -\mathscr{J}(0)\tfrac{1}{2}\langle \boldsymbol{J}_1 + \boldsymbol{J}_2\rangle \cdot \boldsymbol{J}_1 - \mathscr{J}(Q)\tfrac{1}{2}\langle \boldsymbol{J}_1 - \boldsymbol{J}_2\rangle \cdot \boldsymbol{J}_1 \\ & - \mathscr{J}_{\mathrm{D}}\tfrac{1}{2}\langle J_{y,1} - J_{y,2} + J_{z,1} - J_{z,2}\rangle J_{x,1} \\ & + \langle J_{x,1} - J_{x,2} + J_{z,1} - J_{z,2}\rangle J_{y,1} + \langle J_{x,1} - J_{x,2} + J_{y,1} - J_{y,2}\rangle J_{z,1}] \\ & - K(0)\sum_m (-1)^m \tfrac{1}{2}\langle \tilde{O}_{2,m}(\boldsymbol{J}_1) + \tilde{O}_{2,m}(\boldsymbol{J}_2)\rangle\, \tilde{O}_{2,-m}(\boldsymbol{J}_1) \\ & - K(Q)\sum_m (-1)^m \tfrac{1}{2}\langle \tilde{O}_{2,m}(\boldsymbol{J}_1) - \tilde{O}_{2,m}(\boldsymbol{J}_2)\rangle\, \tilde{O}_{2,-m}(\boldsymbol{J}_1) \end{aligned} \quad (3)$$

expressed in terms of the acoustic and optical coupling parameters, defined by

$$\begin{aligned}\mathscr{J}(0) &= \sum_j \mathscr{J}(\boldsymbol{r}_i - \boldsymbol{r}_j) \simeq 12\mathscr{J}(\boldsymbol{r}_1) + 6\mathscr{J}(\boldsymbol{r}_2) \\ \mathscr{J}(Q) &= \sum_j \mathscr{J}(\boldsymbol{r}_i - \boldsymbol{r}_j)\exp[\mathrm{i}\boldsymbol{Q} \cdot (\boldsymbol{r}_i - \boldsymbol{r}_j)] \simeq -6\mathscr{J}(\boldsymbol{r}_2).\end{aligned} \quad (4)$$

$\boldsymbol{Q}$ is the wavevector describing the two-sublattice structure of the alternating (111) planes perpendicular to $\boldsymbol{Q}$, and only the couplings between the twelve nearest neighbours, $\mathscr{J}(\boldsymbol{r}_1)$, and the six next-nearest neighbours, $\mathscr{J}(\boldsymbol{r}_2)$, are retained. Similar expressions are valid for $K(0)$ and $K(Q)$, whereas $\mathscr{J}_{\mathrm{D}}(0)$ vanishes due to the cubic symmetry, although $\mathscr{J}_{\mathrm{D}} = \mathscr{J}_{\mathrm{D}}(Q)$ is non-zero. The MF Hamiltonian for $\boldsymbol{J}_2$ belonging to the other sublattice is obtained from (2) and (3) by interchanging the indices 1 and 2. We note that the reduced symmetry of the two-sublattice structure allows one more quadrupole term in (3), which, however, is similar to $K'(Q)$ and therefore can be ignored in HoSb.

In writing the anisotropic dipolar term in (3) we have made a particular choice for $\boldsymbol{Q}$, namely $\boldsymbol{Q} = \pm(\pi/a)(1, 1, 1)$, where $a$ is the lattice parameter. The part $\mathscr{J}_{\mathrm{D}}^0$ of $\mathscr{J}_{\mathrm{D}}$, due to the pure magnetic dipole coupling, is determined from

$$\mathscr{J}_{\mathrm{D}}^0(\boldsymbol{r}_i - \boldsymbol{r}_j) = (g\mu_{\mathrm{B}})^2 |\boldsymbol{r}_i - \boldsymbol{r}_j|^{-3}.$$

The lattice sums of the long-range dipole coupling at different wavevectors have been calculated by Cohen and Keffer (1955). In the present case

$$\mathscr{J}_{\mathrm{D}}^0(Q) = [(g\mu_{\mathrm{B}})^2/a^3](-12\sqrt{2} + 0 + 8\sqrt{6/9} + 3\sqrt{2/2} + \ldots) = -14{\cdot}46(g\mu_{\mathrm{B}})^2/a^3 \quad (5)$$

or $-5{\cdot}28 \times 10^{-3}$ meV ($a = 6{\cdot}13$ Å or $N = 1{\cdot}74 \times 10^{22}$ Ho ions cm$^{-3}$). Besides the microscopic dipole field the coupling also gives rise to the macroscopic Lorentz field (and the demagnetisation effects included in the internal field). It is easily seen that the Lorentz field only adds to the effective value of $\mathscr{J}(0)$ by $\frac{4}{3}\pi N(g\mu_B)^2$, equal to $6{\cdot}13 \times 10^{-3}$ meV.

In the numerical calculations the MF Hamiltonian of the sublattice 1 is diagonalised, determining the $(2J + 1)$ eigenvalues $\mathscr{E}_\nu$ and the corresponding eigenfunctions $|\nu\rangle$. The thermal expectation value of an operator $A$ is

$$\langle A\rangle = \frac{1}{Z_1}\sum_{\nu=1}^{2J+1}\langle\nu|A|\nu\rangle\exp(-\mathscr{E}_\nu/k_BT) \tag{6a}$$

where

$$Z_1 = \sum_{\nu=1}^{2J+1}\exp(-\mathscr{E}_\nu/k_BT) \tag{6b}$$

and the free-energy per ion belonging to sublattice 1 is

$$F_1 = -k_BT\ln Z_1.$$

The same scheme is applied to an ion belonging to the other sublattice. The (new) expectation values determined by (6) are introduced in (3), and the calculations are repeated until a self-consistent solution is attained. Except close to second-order phase transitions convergence is rapid. When comparing different solutions to these equations, the phase having the lowest free-energy per ion, $F = \frac{1}{2}(F_1 + F_2)$, was chosen, as it is the most stable one. We note that, in such a comparison, it is important to include the last, 'constant' term in (2). The procedure used here is equivalent to the one applied for the seven/eight sublattice structure calculation for Er (Jensen 1976).

To illustrate the effects of the different two-ion parameters, we consider the free-energy $F$ at $T = 0$, using the simplifying crystal-field model of $x = x_c$. The crystal-field energies of the three different phases occurring when the field is applied along a [100] direction are equal, whereas the two-ion and Zeeman contributions differ. The calculation is straightforward and the two critical fields are given by

$$\begin{aligned} H_1^* + H_2^* &\simeq cJ[\mathscr{J}(Q) - \mathscr{J}(0)]/g\mu_B \\ H_2^* - H_1^* &\simeq cJ\{-\mathscr{J}_D + \tfrac{3}{2}[K(Q) - K(0)](J - \tfrac{1}{2})^2\}/g\mu_B. \end{aligned} \tag{7}$$

The mean value of the two fields is determined by the isotropic exchange interaction, whereas the flopside structure is stable ($H_2^* > H_1^*$) only because of the anisotropic couplings. The dipole contribution, (5), to $\mathscr{J}_D$ is negative and contributes in HoSb to $H_2^* - H_1^*$ by 5·8 kOe, which is to be compared with the experimental value of about 7 kOe (see figure 4).

Because of certain effects discussed later on we shall not assume that $K(Q) - K(0)$ is negligible, but instead assume that the electronic contribution, $K_{el}(0)$, to $K(0)$ can be neglected. Then $K(0)$ is solely of magnetoelastic origin. In general, it is not possible to distinguish between intrinsic, electronic quadrupolar terms in the MF Hamiltonian and the crystal-field terms introduced by strain. An exception to this is that the magnetoelastic contributions to $K(0)$ or $K(Q)$ are *always* non-negative, whereas there is no such constraint on the electronic terms.

The magnetoelastic part, $K_{me}(0)$, of $K(0)$ is determined from the induced strain, $\Delta l/l$, parallel to a field applied along a [001] direction in the paramagnetic phase of

HoSb. In figure 7 is shown the experimental result reported by Lüthi *et al* (1977) compared with the calculated behaviour

$$\Delta l/l = \epsilon_{33} = (\pm)\{[2N/3(c_{11} - c_{12})]K_{me}(0)\}^{1/2}\langle\tilde{O}_{2,0}\rangle. \tag{8}$$

The field is assumed to be in the $z$ direction, $\tilde{O}_{2,0} = \frac{1}{2}[3J_z^2 - J(J+1)]$, and at these temperatures the two sublattices are identical. The value of $K_{me}(0)$ determined by this fit is the same as that deduced by Mullen *et al* (1974) from the temperature dependence of

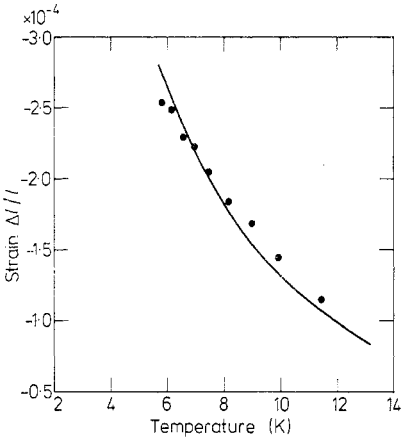


**Figure 7.** The magnetoelastic strain, $\Delta l/l$, induced parallel to a field of 15 kOe applied along a [001] direction in the paramagnetic phase of HoSb. The experimental results are those reported by Lüthi *et al* (1977).

$c_{11} - c_{12}$ in HoSb. By definition $K_{me}(0)$ is equal to $4g_2^2$ in their notation, and the isotropy relation, i.e. $K_{me}(0) = -K'_{me}(0)$, corresponds to $g_2^2$ being equal to $\frac{1}{3}g_3^2$. The expression (8) has a general validity, but in order to reduce the number of parameters, we assume that

$$K(0) = K_{el}(0) + K_{me}(0) \simeq K_{me}(0).$$

The remaining six parameters, four two-ion and two single-ion, occurring in the MF Hamiltonian, (2) and (3), can now be determined from the experiments.

The two crystal-field parameters and $\mathcal{J}(0)$ determine the paramagnetic susceptibility of $Ho_cY_{1-c}Sb$

$$\chi^c(0) = \chi_0/[1 - c\mathcal{J}(0)\chi_0] \tag{9}$$

where $\chi_0$ is the non-interacting susceptibility as given by for instance Bak and Lindgård (1973). For convenience, $\chi$ in this section is defined in units of $(g\mu_B)^2$. The three parameters also determine the high-field magnetisation in the ordered phase, and the crystal field is important for the variation of $T_N$ with $c$. For instance, if $x$ were equal to $x_c$ then $T_N$ as a function of $c$, in figure 6, would be a straight line through the origin. The final values of the fitting parameters are given in table 1, and in figure 8 we compare our values for the reduced crystal-field parameters, $A_4\langle r^4\rangle = B_4^0/\beta_J$ and $A_6\langle r^6\rangle = B_6^0/\gamma_J$, with those determined in other rare-earth antimonides. The crystal-field parameters deduced correspond to $x = 0{\cdot}70$ and $W = -0{\cdot}23$ K in the notation of Lea *et al* (1962) which implies a level scheme having the non-magnetic doublet, $\Gamma_3^{(2)}$, as ground state. The splitting between the ground state and the $\Gamma_4^{(2)}$ triplet is 3·44 K, and the $\Gamma_1$ singlet lies

**Table 1.** The MF parameters of HoSb (in meV) as defined in the text. These values for the parameters are used in all the calculated results given by the full curves in the figures.

| Parameter | Value |
|---|---|
| $B_4^0$ | $(-2{\cdot}3 \pm 0{\cdot}15) \times 10^{-4}$ |
| $B_6^0$ | $(-4{\cdot}3 \pm 0{\cdot}8) \times 10^{-7}$ |
| $\mathcal{J}(0)$ | $(-1{\cdot}19 \pm 0{\cdot}1) \times 10^{-2}$ |
| $\mathcal{J}(Q)$ | $(2{\cdot}17 \pm 0{\cdot}1) \times 10^{-2}$ |
| $\mathcal{J}_D$ | $-2{\cdot}0 \times 10^{-3}$ |
| $K(0)$ | $3{\cdot}73 \times 10^{-5}$ |
| $K(Q)$ | $9{\cdot}33 \times 10^{-5}$ |

12·0 K above the ground state. The remaining levels all lie at much higher energies (90–125 K). With this level scheme the inverse single-ion susceptibility, $1/\chi_0$, is very close to a linear function of $T$ between 10–300 K, in accordance with the experiments. The slight curvature of $1/\chi_0$ causes uncertainties in the calculated values of $P_{\text{eff}}^2 = c(113{\cdot}1 \pm 0{\cdot}1)$ and $\theta_p = -(1{\cdot}53 \pm 0{\cdot}1)$ K in the limit of $c = 0$. Because the ground state is non-magnetic, $\chi_0$ starts to saturate at low temperatures (below 10 K) as shown in figure 1.

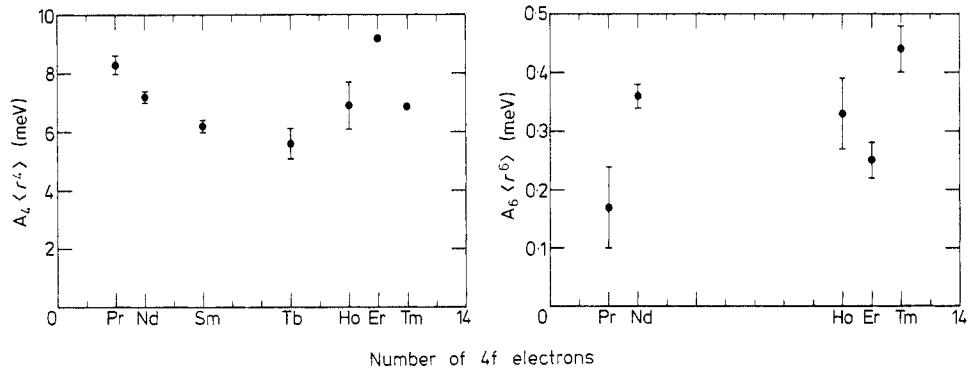


**Figure 8.** The reduced crystal-field parameters, $A_4\langle r^4\rangle = B_4^0/\beta_J$ and $A_6\langle r^6\rangle = B_6^0/\gamma_J$, determined in various rare-earth antimonides, and displayed according to the number of 4f electrons of the rare-earth ions.

The results are obtained from: Pr: Turberfield *et al* (1971); Nd: Furrer *et al* (1972); Sm: Mullen *et al* (1974); Tb: Stutius 1969); Ho: this work; Er: Shapiro and Bak (1975); Tm: Birgeneau *et al* (1971).

The anisotropic bilinear coupling, $\mathcal{J}_D$, does not affect the paramagnetic susceptibility at zero wavevector, but the staggered susceptibility is anisotropic

$$\chi_\perp^c(Q) = \frac{\chi_0}{1 - c[\mathcal{J}(Q) - \mathcal{J}_D]\chi_0} \qquad \chi_\parallel^c(Q) = \frac{\chi_0}{1 - c[\mathcal{J}(Q) + 2\mathcal{J}_D]\chi_0} \tag{10}$$

where $\perp$ or $\parallel$ indicates the component perpendicular or parallel to $\boldsymbol{Q}$. The signs of the dipole contribution, $\mathcal{J}_D^0$, and of $H_2^* - H_1^*$ both indicate that $\mathcal{J}_D$ is negative, and therefore that $\chi_\perp^c(Q) > \chi_\parallel^c(Q)$. Considering only this possibility, the divergence of $\chi_\perp^c(Q)$ at the temperature $T_N$, determined by

$$c(\mathscr{J}(Q) - \mathscr{J}_D)\chi_0(T = T_N) = 1 \tag{11}$$

implies the presence of a magnetically ordered phase below this temperature. There exist two possibilities, either that a second-order magnetic transition occurs at $T_N$, or that the magnetic ordering is already finite at this temperature, in which case the transition to the paramagnetic phase at higher temperatures is of first order. In the case of the second-order transition the ordered phase, just below $T_N$, is antiferromagnetic, $\boldsymbol{Q} = (\pi/a)$ (1, 1, 1) or the equivalent choices, with the moments lying in the (111) plane perpendicular to $\boldsymbol{Q}$. The possible existence of a quadrupolar ordered phase above $T_N$ can be included by determining $\chi_0$ in the presence of the quadrupolar field. The various possibilities have been discussed extensively by Uffer *et al* (1974) and Kim *et al* (1975, 1976) in the ferro-

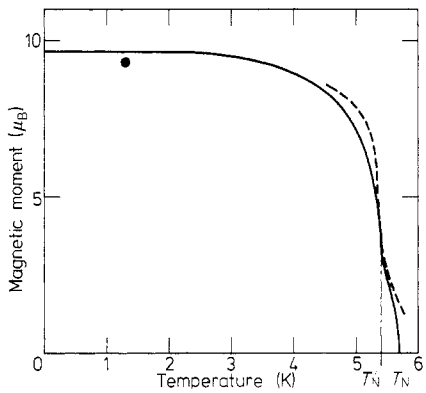


**Figure 9.** The sublattice magnetisation, $|\mu|$, of HoSb calculated as a function of temperature. The broken line shows the experimental results deduced from the intensity, $I$, of magnetically scattered neutrons at the wavevector $(\pi/a)$ (1, 1, 1) as measured by Taub and Parente (1975), $|\mu| \propto \sqrt{I}/\sin\psi$. Close to $T_N$ these results include the effect of critical scattering of the neutrons. The full circle denotes the low-temperature result of Child *et al* (1963).

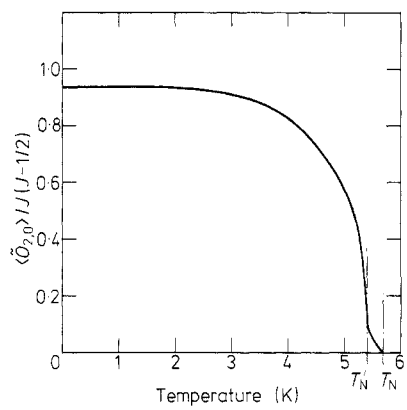


**Figure 10.** The temperature dependence of $\langle\tilde{O}_{2,0}\rangle/J(J-\frac{1}{2})$ calculated in HoSb. The quadrupole moments of the two sublattices are equal. The $z$ axis is fixed to be along the [001] direction defined in figure 11 in relation to the angle $\psi$. This choice implies that $\langle\tilde{O}_{2,2} + \tilde{O}_{2,-2}\rangle$ vanishes identically, and the remaining off-axis components are all very small.

magnetic case which is equivalent to the antiferromagnetic one if $\mathscr{J}_D$ vanishes. Neglecting quadrupolar couplings they find that if $x = x_c$ then the transition is just at the borderline between a first- and a second-order transition, i.e. the system is tricritical at $T = T_N$. When $K(0)$ is finite they determined the transition to be of second order if $K(0)$ is negative, but of first order if $K(0)$ is positive (Kim *et al* 1975). $K(0)$ contributes to the energy of both the ferro- and antiferromagnetic phases, whereas the term due to $K(Q)$ vanishes in these structures. In the present case $x$ is slightly less than $x_c$ which necessitates a few modifications (see also Kim *et al* 1976). Again neglecting $K(0)$ and $\mathscr{J}_D$ we find the transition to be of second order in the Ho-rich alloys, but of first order when the ordering temperature is below about 1·3 K. In the dilute limit the non-magnetic crystal-field ground state destroys the tendency for magnetic ordering. The introduction of $K(0)$ equal to $K_{me}(0)$, which is positive, causes the transition in HoSb to be of first order with a discontinuous change of the moments by about $6\mu_B$ (see also Uffer *et al* 1974). Such a strong first-order behaviour

is not consistent with the neutron diffraction measurements of Taub and Parente (1975). However, the introduction of a finite $\mathcal{J}_D$ has important consequences on the phase transition in the antiferromagnetic case, as suggested by the appearance of $\mathcal{J}_D$ in (10) and (11). In fact, choosing $\mathcal{J}_D$ equal to $-2{\cdot}0 \times 10^{-3}$ meV gives a temperature dependence of the magnetisation which is very close to that determined from the experiment of Taub and Parente. In figure 9 we show our final results for the sublattice magnetisation in HoSb as a function of $T$, compared with the square root of the intensity of magnetically scattered neutrons at wavevector $\boldsymbol{Q}$ (Taub and Parente 1975). The similarities between the calculated and experimental behaviour are striking, and the minor differences are to be expected as an inherent effect of the MF approximation. This agreement allows us to put confidence in the behaviour predicted by the present MF model for HoSb. The theoretical model predicts a second-order transition at $T_N = 5{\cdot}70$ K followed by a very steep increase of the magnetisation around $T_N' = 5{\cdot}4$ K. In the interpretation of their results Taub and Parente associate the temperature $T_N'$ with the ordering temperature, and the magnetic intensity above this temperature they considered to be due to an anomalously large critical scattering. Associated with the transition at $T_N'$ they observed a modification, due to a magnetoelastic strain, of the nuclear (111) reflection, which in our model is consistent with the strong increase of $\langle \tilde{O}_{2,0} \rangle$ occurring at this temperature and shown in figure 10.

Taub and Parente could not detect any discontinuous change of the order parameter in HoSb. Further, Mullen *et al* (1974) observed a 40% softening of $c_{11} - c_{12}$ close to $T_N$, which indicates that the transition is (close to) second order. The strong modification of $c_{11} - c_{12}$ occurring in the paramagnetic phase can be explained in a random-phase (RPA) model only by the introduction of a strong electronic enhancement of the quadrupole susceptibility, and in their analysis Mullen *et al* deduced a $(g')^2$ corresponding to a value of $K_{el}(0)$ five to six times larger than $K_{me}(0)$. In the paramagnetic phase time-reversal symmetry implies that the magnetic contribution to a quadrupole susceptibility at zero frequency vanishes within RPA. However, this argument does not eliminate higher-order magnetic contributions and close to a second-order magnetic transition the critical fluctuations limit the usefulness of the RPA. In fact, the situation just below $T_N$ in HoSb has the easy-plane resemblance to the HCP ferromagnet Tb, in which case $c_{66}$ is finite only because of the hexagonal anisotropy (Jensen and Palmer 1979). The symmetry differs in the two cases, for instance the $c_{11} - c_{12}$ and the $c_{44}$ modes should be affected in a related way by the magnetic ordering in HoSb, but the mixing with the $c_{44}$ mode is strongly opposed by the large anisotropy of the quadrupole susceptibility. The three-fold axis normal to a (111) plane implies that only $B_6^0$ gives rise to a very small anisotropy within this plane, the negative sign of $B_6^0$ favouring a $[\bar{1}\bar{1}2]$ direction. In contrast, $B_4^0$ produces an anisotropy field tending to pull the moments out of the (111) plane towards a [001] axis. The symmetry of the magnetic phase just below $T_N$ predicted by our model indicates that $c_{11} - c_{12}$ might be strongly reduced due to magnetic effects, which should also be reflected in the behaviour above $T_N$. We therefore propose that the softening of $c_{11} - c_{12}$ in HoSb close to $T_N$, is due to critical magnetic fluctuations rather than to a large electronic quadrupole coupling. In fact, the large value of $K_{el}(0)$ deduced by Mullen *et al* (1974) from the temperature dependence of $c_{11} - c_{12}$ is incompatible with the present analysis.

Because of the crystal field the angle $\psi$, between the direction of the magnetic moments and the [111] axis, changes with temperature. $\psi$ starts to deviate from 90° immediately below $T_N$, due to the effect of $B_4^0$ mentioned above. As shown in figure 11, $\psi$ changes rather abruptly at $T_N'$. This rapid variation of $\psi$ may serve as the most precise definition

of $T'_N$. Within the accuracy of the numerical calculations no discontinuous change of $\psi$ was detected, but a precise determination of the nature of this transition is difficult to achieve. Below $T'_N$ the magnetic moments still make a finite angle with the [001] direction, but this becomes very small, $\sim 2°$, below 3 K. At all temperatures the moments are confined to the plane defined by the $[\bar{1}\bar{1}2]$ and [001] axes. This confinement is mainly due to $B_4^0$, and as mentioned above it is very weak close to $T_N$. The calculated temperature

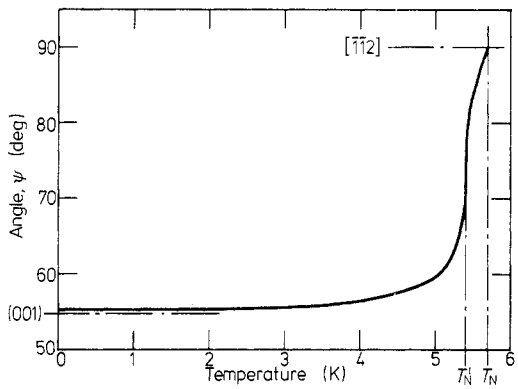


**Figure 11.** The angle $\psi$ between the direction of the magnetic moments (in one of the two sublattices) and $\boldsymbol{Q}$, chosen to be along [111], calculated as a function of temperature in HoSb. At all temperatures the magnetic moments are confined to the plane defined by the $[\bar{1}\bar{1}2]$ and [001] directions corresponding to $\psi$ being equal to 90° and 54·74° respectively. $T'_N$ is considered to be defined by the abrupt change of $\psi$ displayed on the figure. The position of this transition is also marked on the preceding figures 9 and 10.

dependence of the magnetisation vector in HoSb, which is given by figures 9 and 11, is very similar to that of DySb determined from neutron diffraction measurements by Felcher *et al* (1973). DySb and HoSb have many features in common, the most significant difference being that $K(0)$ is relatively larger in DySb, so that the transition at $T'_N$ is instead a first-order transition between the paramagnetic and antiferromagnetic regimes. Felcher *et al* proposed that the unusual behaviour of the magnetic moment in DySb is produced by the dipole coupling, in agreement with the present model (see also the abstract by Rhagavan and Levy 1979).

In the fit we use the indication from the neutron data in figure 9 that $T'_N$ is 5·4 K. $T_N$ is considered to be determined partly by these data and partly by the results given in figure 6, which presumably reflect the transition at $T_N$ rather than the one at $T'_N$. Using $K(0) = K_{me}(0)$, then $T'_N$ and $T_N$ determine the values of $\mathcal{J}_D$ and $\mathcal{J}(Q)$. Of the three parameters $\mathcal{J}(Q)$ is the most important one in determining $T_N$ as a function of $c$, which is shown in figure 6. According to the general discussion above, the change in nature of the magnetic transition occurring at $c = c_T \simeq 0{\cdot}34$ is an effect of the $\Gamma_3^{(2)}$ doublet ground state rather than of $\mathcal{J}_D$ or $K(0)$. At the concentration $c = c_T$, $T_N$ and $T'_N$ coincide and this system is tricritical. In contrast to the dipole susceptibility, the quadrupole susceptibility of the operator $\tilde{O}_{2,0}$(or $\tilde{O}_{2,\pm 2}$) includes elastic contributions from the $\Gamma_3^{(2)}$ ground state, which implies that it diverges in the zero-temperature limit. Eventually, at low concentrations, a second-order transition to a phase having a non-zero quadrupole moment occurs at $T_Q$ before the magnetic transition. If $T_N$ is larger than $T_Q$ this phase is quenched,

whereas the presence of a finite quadrupole moment has no essential implications for the magnetic transition. We find $K(Q)$ to be larger than $K(0)$ implying that the quadrupolar phase, indicated on figure 6, is characterised just below $T_Q$ by a non-zero $\langle \tilde{O}_{2,0} \rangle$ the sign of which is opposite in the two different (111) planes.

At low temperatures both $\langle J_z \rangle$ and $\langle \tilde{O}_{2,0} \rangle$ are close to their saturation values in HoSb, and the calculated moment of $9{\cdot}64\mu_B$ at zero temperature agrees reasonably with the low-temperature result of $9{\cdot}3\mu_B$ reported by Child *et al* (1963). Figure 12 shows the

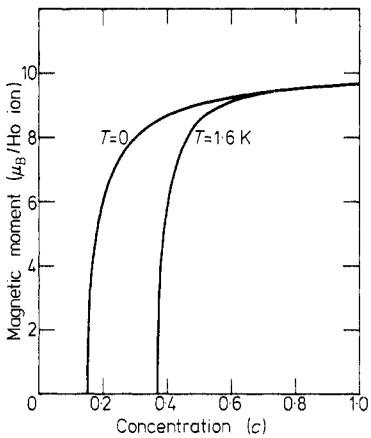


**Figure 12.** The sublattice moment of $Ho_cY_{1-c}Sb$ per Ho ion calculated as a function of $c$ at 1·6 K and at zero temperature.

calculated dependence on $c$ of the magnetic moment at 1·6 K and at zero temperature. The transitions occurring in the field-dependent bulk magnetisation of HoSb at 1·6 K (figures 4 and 5) fix the parameter $K(Q)$ and also $\mathcal{J}(0)$. The value of $H_1^* + H_2^*$ gives a more accurate determination of $\mathcal{J}(0)$ than that obtainable from the susceptibility measurements. The approximate expressions for the positions of the transitions, (7), are found to be quite closely fulfilled in HoSb. The calculated magnetic structures, occurring when a field is applied in the symmetry directions of HoSb, are similar to those expected on the basis of the $x = x_c$ crystal-field model. The anisotropy field due to $\mathcal{J}_D$ gives rise to slight distortions, which are already present in zero field (see figure 11). More important modifications are due to the deviation of $x$ from $x_c$ and to the finite temperature, raising the possibilities of pulling the moments away from a [001] direction and of reducing their magnitudes. Besides the obvious effects, reflected directly in the magnetisation curves, these extra degrees of freedom were important in the following cases. In the structure calculated at high fields applied in a [111] direction, the moment of one of the two sublattices is directed almost along the [110] axis. The other modification we shall mention is of more significance. It is reflected in the calculated curves in figure 4 for $c$ less than 1 by smearing out the transition at $H_1^*$. Instead of the flopside structure other structures turned out to be possible at the intermediate fields, of which the most important one is described as having the moments of both sublattices parallel to the field, along [001], but one of the moments being of reduced magnitude and, at low fields, directed opposite to the field. This structure allows a greater and smoother variation of the bulk magnetisation than the flopside configuration. It is only metastable when

$c = 1$, but at 0·9 it is the stable one between 10 and 13 kOe, and at the smaller concentrations the (simple) flopside structure ceases to be stable. We shall not present a more detailed account of the different configurations which have been calculated, partly because they depend on the chosen parameters, for instance $K(0) + K(Q)$, which only have minor consequences for the magnetisation parallel to the field. The comparison between the calculated and experimental magnetisation curves in figures 4 and 5 deserves one more comment. The transitions at $H_3^*$ and $H_4^*$ in HoSb are observed to be more sharp than those at $H_1^*$ and $H_2^*$. The more gradual change occurring when the field is along the [001] axis might be due to the presence of metastable configurations of energies just above that of the ground state. The number of low-lying metastable states is limited in the two other cases, and also the difference in free-energy between the stable configurations occurring on either side of one of the transitions depends more rapidly on field around $H_3^*$ and $H_4^*$ than around $H_1^*$ and $H_2^*$.

The final values for the parameters are given in table 1, and all the calculated results, shown by the full curves in the figures, are obtained using these numbers. The experimental evidence is not entirely sufficient to establish the MF model uniquely. The uncertainty is raised by the possible electronic contribution, $K_{el}(0)$ to $K(0)$ which is neglected in the fitting procedure. It is unlikely that $K_{el}(0)$ is negative, but a positive contribution to $K(0)$ of as much as $K_{me}(0)$ itself cannot be excluded. If the value of $K(0)$ is doubled, much the same results are obtained if the values of $\mathcal{J}_D$ and $K(Q)$ in table 1 are multiplied by about 1·4 and 1·3 respectively. The remaining parameters are not very sensitive to this change. If $K(0)$ is increased by more than a factor of two major discrepancies start to develop.

## 4. Discussion

The magnetic properties of $Ho_cY_{1-c}Sb$ are found to be determined by a complex cooperation between the different types of interactions. These might be divided into three main categories: the crystal field, the isotropic exchange, and the anisotropic two-ion interactions. The competitive effects of the crystal field and the exchange coupling are the dominating ones for establishing the phase diagram, the strong confinement of the moments at low temperatures, the paramagnetic susceptibility, etc. Although the anisotropic couplings are an order of magnitude weaker than the isotropic one, they are clearly manifested in the experimental results. The neutron diffraction results of Taub and Parente (1975) for the sublattice magnetisation of HoSb indicates the occurrence of two magnetic transitions, at $T_N$ and $T_N'$, separated by only $\sim 0{\cdot}3$ K in our interpretation. The intermediate phase present in an applied field along a [001] direction in HoSb at 1·6 K can only be accounted for by the anisotropic two-ion interactions. Finally, the magnitude of the magnetoelastic coupling, $K_{me}(0)$, is determined by the experimental results of Mullen *et al* (1974) and Lüthi *et al* (1977).

The fitting procedure, based on the two-sublattice MF Hamiltonian, gives a quite accurate determination of the crystal-field and isotropic exchange parameters, which all compare with those determined in other rare-earth antimonides. With the use of (4), the exchange parameters may be expressed in terms of a ferromagnetic nearest neighbour and an antiferromagnetic next-nearest neighbour coupling which are

$$\mathcal{J}(r_1) = 0{\cdot}82 \times 10^{-3}\,\text{meV} \qquad \mathcal{J}(r_2) = -3{\cdot}62 \times 10^{-3}\,\text{meV}.$$

If the Lorentz dipole-field contribution is subtracted from $\mathcal{J}(0)$, then $\mathcal{J}(r_1)$ is reduced to

$0{\cdot}31 \times 10^{-3}$ meV. We note that the Lorentz field gives rise to an effective ferromagnetic coupling of the different (111) planes within any one of the two sublattices which is more than sufficient for maintaining the two-sublattice structure under all the circumstances considered.

It is not possible to get a precise estimate of the three anisotropy parameters $\mathcal{J}_D$, $K(0)$, and $K(Q)$ without further experimental evidence. The most informative experiment would be a study of the magnetic excitations in HoSb at low temperatures using inelastic neutron scattering. The quality of the fit which is obtained allows us to put a limit on the range over which the parameters may vary. $\mathcal{J}_D$ is certainly smaller than the pure dipole contribution, $\mathcal{J}_D^0$, by a factor lying between two and three. This difference can be produced by the indirect exchange coupling and is compatible with the free-electron estimate of Kaplan and Lyons (1963).

The quadrupole parameters, $K(0)$ and $K(Q)$, are both positive and they are of the same order of magnitude, $K(Q)$ being somewhat larger than $K(0)$. The order of magnitude estimate of the electronic contribution, given in the introduction, suggests terms of the size of $K_{me}(0)$. However, this estimate should not be taken too literally, and these terms might be smaller. At least we find that $K_{me}(0)$ represents the upper limit of $K_{el}(0)$, and further that the magnetoelastic contribution to $K(0)$ is sufficiently large to account for the experiments. In the flopside structure the non-zero quadrupole moments are $\langle \tilde{O}_{2,0}(J_{z'}) \rangle \approx J(J - \frac{1}{2})$, the $z'$ axis being parallel to the magnetic moments on either one of the two sublattices, for example the [100] and [010] directions. A consideration of the strain modes, which are compatible with this configuration, shows that there is one at wavevector $\boldsymbol{Q} = (\pi/a)\,(1, 1, 1)$ induced by $K_{me}(Q)$, the magnetoelastic part of $K(Q)$. In this strain mode the Sb ions are displaced along the $[1\bar{1}0]$ direction, perpendicular to $\boldsymbol{Q}$ and in the plane of the quadrupole moments, corresponding to a normal mode of the lattice, i.e. a transverse phonon at $L$. We emphasise that the polarisation vector of the strain mode is *not* along one of the [001] directions as is sometimes stated. The remaining two orthogonal polarisation vectors, [110] and [001] in our example, are those describing the uniform strain mode induced by $K_{me}(0)$. We may add that the 'optical' quadrupolar phase below $T_Q$ involves the other transverse mode at L of the Sb lattice, i.e. the one polarised along $[11\bar{2}]$. These two phonon modes are degenerate in the case of no ordering. In principle it should be possible to determine $K_{me}(Q)$ by measuring the magnitude, $u_{Sb}$, of the transverse optical displacement of the Sb ions in the flopside configuration which is given by

$$u_{Sb} = \pm[3K_{me}(Q)/4M_{Sb}\omega_{Sb}^2]^{1/2} \langle \tilde{O}_{2,0} \rangle \tag{12}$$

where $M_{Sb}$ is the mass of the Sb ions and $\omega_{Sb}$ is the angular frequency of the transverse phonon mode at L. Using the frequency of $2\pi \times 3{\cdot}25 \times 10^{12}\,s^{-1}$ observed in NdSb (Wakabayashi and Furrer 1976) and $K_{me}(Q) = K(Q)$ we get $u_{Sb} \simeq 1{\cdot}1 \times 10^{-3}\,a \simeq 7 \times 10^{-3}$ Å in HoSb at low temperatures. The simplest model of an isotropic magnetoelastic coupling between nearest neighbouring Ho and Sb ions suggests that

$$K_{me}(Q)\tfrac{1}{6}M_{Sb}\omega_{Sb}^2 a^2 = K_{me}(0)(c_{11} - c_{12})/2N = -K'_{me}(0)c_{44}/N$$

and hence that $K_{me}(Q) \approx 0{\cdot}8\,K_{me}(0)$ should be a factor of three smaller than $K(Q)$.

The positive, acoustic quadrupole coupling $K(0)$, together with the crystal-field interaction, favours an alignment of the (quadrupole) moments along an [001] axis, and it sustains magnetic ordering above $T_N$, determined by (11). These tendencies are opposed by the anisotropic bilinear coupling $\mathcal{J}_D$, because it tends to pull the moments away from the [001] axis towards the (111) plane perpendicular to $\boldsymbol{Q}$. The tilting of the

moments is accompanied by a simultaneous reduction of their magnitude. The relatively slow increase of the magnetisation calculated for HoSb below $T_N$, but above $T'_N$, is due to $\mathcal{J}_D$ (see figure 9). If $\mathcal{J}_D$ is replaced by $\mathcal{J}_D^0$ then the stronger dipole coupling reduces substantially the magnetisation between $T_N$ and down to 2 K, in comparison with the result shown in figure 9. Bak *et al* (1976) have discussed the critical behaviour of systems which have order parameters with $n \geqslant 4$ components. They used Landau symmetry arguments to predict a first-order transition in the case of a type-II antiferromagnet where the magnetic moment lies along a [001] direction, corresponding to HoSb or DySb if $\mathcal{J}_D$ vanishes. If the ordered phase is a type-II antiferromagnet with the moments directed perpendicular to $\boldsymbol{Q}$, as we expect to be the case in HoSb just below $T_N$, then Bak *et al* predict the transition to be of first order instead of the second-order behaviour suggested by the MF approximation. In the latter case the first-order behaviour is dictated not by symmetry arguments but by the absence of a stable fixed point in Wilson's $\epsilon$-expansion of the renormalisation-group equations. In DySb a MF model may easily account for the occurrence of the first-order transition, whereas the MF calculation predicts the transition to be of second order in HoSb, which should therefore be an adequate example for testing the $\epsilon$-expansion hypothesis of Bak *et al* (1976). However, the slow increase of the magnetisation between $T_N$ and $T'_N$ (figure 9) indicates that the presence of a discontinuity in the order parameter close to '$T_N$' might be too small to be detected experimentally, (compare also with the discussion of Taub and Parente 1975).

The magnetic specific heat, $C_M$, has been calculated for HoSb. The MF result exhibits a strong peak centred at $T'_N$. The peak value is found to be finite, but the limited accuracy of the numerical calculations might disguise a possible divergence of $C_M$ at $T'_N$. The effect of the transition at $T_N$ is dominated entirely by the large peak at $T'_N$ (critical fluctuations are not included). This calculated behaviour is in good agreement with the experimental result of Taub and Williamson (1973) and Taub *et al* (1974) who reported a temperature of 5·4 K for the position of the peak, consistent with our interpretation. The calculated values of $C_M$ are slightly smaller than the experimental ones above $T_N$, and the reverse below $T'_N$, which minor differences are characteristic of the MF approximation. The calculation indicates that HoSb is very nearly tricritical at $T'_N$ which is substantiated by the critical exponents $\alpha = 0{\cdot}85$ and $\alpha' = 0{\cdot}54$ determined by Taub *et al* from their measurements of the specific heat and the temperature derivative of the resistivity respectively. These exponents compare with $\alpha = \frac{1}{2}$ applying in the case of a tricritical system (see also the discussion by Uffer *et al* 1974).

There are two aspects which might be relevant in a comparison with the magnetic properties of other rare-earth monopnictides. One is the determination of the strength of the different interactions in HoSb, which should be comparable in other rare-earth antimonides, with appropriate scaling. To some extent this might also apply to the other monopnictides. The other is the presentation of two examples in which the anisotropic two-ion forces are crucial. We have already discussed the implication of the comparison between our model for HoSb and the temperature dependence of the sublattice magnetisation in DySb. The different couplings in HoP are presumably very close in magnitude with those occurring in HoSb, with one exception. The stability of the flopside structure in zero field and at low temperatures requires that the parameters of HoP give a negative value for $H_1^*$ and a positive one for $H_2^*$ when inserted in equation (7). The transition temperature in HoP is 5·5 K, which is about the same as in HoSb, and this is probably also the case with the anisotropy field, $H_2^* - H_1^*$. Therefore we expect that the only significant difference between HoSb and HoP is a change of $\mathcal{J}(0)$ so that $\mathcal{J}(0) \approx \mathcal{J}(Q)$ in HoP. A definitive model for the anisotropy field in HoP requires studies

like those we have performed on HoSb or an extension of the neutron scattering experiments of Furrer *et al* (1975, 1977). As first proposed by Trammell (1963) the magnetic dipole force might be sufficient for stabilising the flopside structure in HoP.

## Acknowledgments

It is a pleasure to thank R Gubser, Institut für Kristallographie und Petrographie der ETHZ, Zürich for performing the electron microprobe analysis, L Scherrer and K Mattenberger for technical assistance and A R Mackintosh for a critical reading of the manuscript. Stimulating discussions with R Raghavan and P M Levy are much appreciated. One of the authors (NHA) would like to express his gratitude for the hospitality shown him at the Laboratorium für Festkörperphysik, ETH, Zürich during the experimental stages of this work.

## References

Bak P, Krinsky S and Mukamel D 1976 *Phys. Rev. Lett.* **36** 52–5
Bak P and Lindgård P A 1973 *J. Phys. C: Solid St. Phys.* **6** 3774–84
Birgeneau R J, Bucher E, Passell L and Turberfield K C 1971 *Phys. Rev.* B **4** 718–25
Child H R, Wilkinson M K, Cable J W, Koehler W C and Wollan E O 1963 *Phys. Rev.* **131** 922–31
Cohen M H and Keffer F 1955 *Phys. Rev.* **99** 1128–34
Felcher G P, Brun T O, Gambino R J and Kuznietz M 1973 *Phys. Rev.* B **8** 260–5
Furrer A and Kaldis E 1975 *AIP Conf. Proc. No.* **29** 264–5
Furrer A, Kjems J and Vogt O 1972 *J. Phys. C: Solid St. Phys.* **5** 2246–58
Furrer A, Levy P M, and Kaldis E 1977 *Crystal Field Effects in Metals and Alloys* ed A Furrer (New York: Plenum) pp 24–30
Hessel Andersen N, Jensen J, Smith H, Splittorff O and Vogt O 1979a *Phys. Rev.* to be published
Hessel Andersen N, Jensen J and Vogt O 1979b *J. Magn. Magn. Mater.* to be published
Hessel Andersen N and Vogt O 1979 *J. Physique* **40** C5 116–8
Jensen J 1976 *J. Phys. F: Metal Phys.* **6** 1145–59
Jensen J and Palmer S B 1979 *J. Phys. C: Solid St. Phys.* **12** 4573–84
Kaplan T A and Lyons D H 1963 *Phys. Rev.* **129** 2072–86
Kim D, Levy P M and Sudano J J 1976 *Phys. Rev.* B **13** 2054–65
Kim D, Levy P M and Uffer L F 1975 *Phys. Rev.* B **12** 989–1004
Lea K R, Leask M J M and Wolf W P 1962 *J. Phys. Chem. Solids* **23** 1381–405
Lindgård P A and Danielsen O 1974 *J. Phys. C: Solid St. Phys.* **7** 1523–35
Lüthi B, Wang P S, Wong Y H, Ott H R and Bucher E 1977 *Crystal Field Effects in Metals and Alloys* ed A Furrer (New York: Plenum) pp 104–13
Mullen M E, Lüthi B, Wang P S, Bucher E, Longinotti L D, Maita J P and Ott H R 1974 *Phys. Rev.* B **10** 186–99
Rhagavan R and Levy P M 1979 *Bull. Am. Phys. Soc.* **24** 302
Shapiro S M and Bak P 1975 *J. Phys. Chem. Solids* **36** 579–81
Stutius W 1969 *Phys. Kond. Mater.* **9** 341–4
Taub H and Williamson S J 1973 *Solid St. Commun.* **13** 1021–5
Taub H, Williamson S J, Reed W A and Hsu F S L 1974 *Solid St. Commun.* **15** 185–9
Taub H and Parente C B R 1975 *Solid St. Commun.* **16** 857–60
Trammell G T 1963 *Phys. Rev.* **131** 932–48
Turberfield K C, Passell L, Birgeneau R J and Bucher E 1971 *J. Appl. Phys.* **42** 1746–54
Uffer L F, Levy P M and Sablik M J 1974 *Solid St. Commun.* **15** 191–4
Wakabayashi N and Furrer A 1976 *Phys. Rev.* B **13** 4343–7